RSC Advances

PAPER

View Article Online
View Journal | View Issue

Cite this: *RSC Adv.*, 2020, **10**, 15523

Fused tetracyclic tris[1,2,4]triazolo[1,3,5]triazine as a novel rigid electron acceptor for efficient thermally activated delayed fluorescence emitters†

Suraj Kumar Pathak,[ab] Yepeng Xiang,[c] Manli Huang,[c] Taian Huang,[a] Xiaosong Cao,[a] He Liu,*[a] Guohua Xie[c] and Chuluo Yang*[ac]

Received 29th February 2020
Accepted 4th April 2020

DOI: 10.1039/d0ra01925a

rsc.li/rsc-advances

Tris[1,2,4]triazolo[1,3,5]triazine, a new acceptor based on a fused triazole and triazine moiety, is utilized to construct D_3–A star-shaped tristriazolotriazine derivatives, named 3,7,11-tris(4-(10*H*-phenoxazin-10 yl) phenyl)tris([1,2,4]triazolo)[1,3,5]triazine (**TTT-PXZ**) and 3,7,11-tris(4-(9,9-dimethylacridin-10(9*H*)yl)phenyl) tris([1,2,4])triazolo[1,3,5]triazine (**TTT-DMAC**). Both **TTT-PXZ** and **TTT-DMAC** emitters feature TADF activities and AIEE properties. Consequently, solution processed OLEDs based on **TTT-PXZ** green emitters exhibited good performances, with an external quantum efficiency (EQE) of up to 6.2%.

Introduction

Metal free thermally activated delayed fluorescence (TADF) has attracted substantial attention from the scientific community due to its competence of utilizing both singlet and triplet excitons for light emission.[1–7] The seminal work of Adachi *et al.*[2] elucidating the up conversion of a triplet exciton into a singlet state *via* a reverse intersystem crossing (RISC) process by regulating the singlet–triplet splitting energy (ΔE_{ST}), provided new prospects in the field of TADF research, with a bright future in the area of organic light emitting diodes (OLEDs). To realize efficient TADF materials from the quantum theory perspective, the spatial separation of electron densities of the highest occupied molecular orbital (HOMO) and lowest unoccupied molecular orbital (LUMO) in one single molecule is needed to acquire a near-zero ΔE_{ST}; and consequently to realize an efficient RISC process.[1–3] In addition, sufficiently high photoluminescent quantum yield (PLQY) is also important to ensure maximumly transition of excitons to photons. The design principles of twisted donor–acceptor (D–A) molecular structure generally depend on bulky substituents or a spiro-junction to realize a small ΔE_{ST} and reinforce the rigidity of the molecular structure leading to the suppression of non-radiative decay.[4] Therefore, in designing TADF molecular structure, carefully choosing donor and acceptor moieties as well as spacer between them are utmost important.

Recently, a renewed interest for star-shaped emitters (D_3–A) to be used in OLEDs arises.[5–7] In general, star-shaped molecules are of many advantages over their linear analogues as they encompass both the character of small molecules and polymers with well-defined molecular structure, superior chemical purity as well as good solution processability.[8–15] There are several examples of fluorene containing star-shaped molecules showing improved device characteristics in comparison to the linear molecules.[8,11–13] Besides, star-shaped D_3–A twisted molecules can reduce intermolecular interaction in the solid state, resulting enhanced solid-state emission with better film forming ability.[14,15] The solution processability and film forming ability encourage these materials to be used in solution processed OLEDs, which is economically feasible for low cost and large-area displays.[16–26] Therefore, it is highly fascinating to develop molecular design to increase the luminescence efficiency and stability of solution-processed OLEDs, specifically on star-shaped TADF emitters. Generally, planar star-shaped molecule has an inherent problem of aggregation-caused quenching (ACQ) due to its planar intermolecular π–π stacking which is a glaring problem in decreasing the luminescence efficiency in solid state.[27,28] Fortunately, the twisted D–A design strategy not only helps in rendering TADF features but also supports the integration of aggregation-induced enhanced emission (AIEE) features in the star-shaped molecules.[29] In addition, star-shaped emitters having multiple D–A transitional channels can sustain large transitional integral for a high radiative rate. Thus, *via* wisely choosing different cores and branches in the star-shaped molecules, the photophysical, optoelectronic and thermal properties can be easily tuned. However symmetrical star-shaped TADF emitters were scarcely reported.[5,6,30]

[a]*Guangdong Research Center for Interfacial Engineering of Functional Materials, Shenzhen Key Laboratory of Polymer Science and Technology, College of Materials Science and Engineering, Shenzhen University, Shenzhen 518060, P. R. China. E-mail: liuhe001@szu.edu.cn; clyang@szu.edu.cn*

[b]*Key Laboratory of Optoelectronic Devices and Systems of Ministry of Education and Guangdong Province, College of Optoelectronic Engineering, Shenzhen University, Shenzhen 518060, P. R. China*

[c]*Hubei Key Lab on Organic and Polymeric Optoelectronic Materials, Department of Chemistry, Wuhan University, Wuhan, 430072, P. R. China. E-mail: clyang@whu.edu.cn*

† Electronic supplementary information (ESI) available: ^{1}H NMR, ^{13}C NMR, TGA, DSC, CV, UV, fluorescence. See DOI: 10.1039/d0ra01925a

Among efficient TADF materials, diverse electron deficient cores based on nitrogen heterocycles including triazine,[5,30] oxadiazole,[7] triazole,[7] pyridine,[31] pyrimidine,[32] quinoxaline,[33] pyrazine[33] and heptazine[34] have been utilized as acceptors. However, electron-acceptor moieties with a strong electron-withdrawing ability are far from sufficient. Heptazine was the latest included in the nitrogen heterocyclic family having seven sp^2 hybridized nitrogen atoms in the fused ring, used as an acceptor in orange-red TADF emitter with high EQE_{max} of 17.5%.[26] Tris[1,2,4]triazolo[1,3,5]triazine (**TTT**) is another heterocycle based on fused triazole and triazine moiety with nine sp^2 hybridized nitrogen atoms and a C_3 symmetry[5–7,30–33,35–40] which can provide an striking and remarkable alternative. It can be considered as a strong acceptor unit for the construction of donor acceptor (D_3–A) TADF structure because of its rigid large electron deficient plane. Recently our group reported an emitter based on fused rigid acridine donor moiety with high PLQY and EQE,[41] indicating fused structure can strengthen the rigidity of the emitters and ultimately increases the radiative luminescence efficiency. Based on aforementioned strategy, fused tetracyclic tris[1,2,4]triazolo[1,3,5]triazine core was used as an rigid acceptor in uncharted territory of donor–acceptor charge transfer emitter.

Considering all these aspects, we report a new kind of star-shaped D_3–A type tris[1,2,4]triazolo[1,3,5]triazine based molecules, named 3,7,11-tris(4-(10*H*-phenoxazin-10-yl)phenyl) tris([1,2,4]triazolo)[1,3,5]triazine (**TTT-PXZ**) and 3,7,11-tris(4-(9,9-dimethylacridin-10(9*H*)-yl)phenyl)tris([1,2,4]triazolo)[1,3,5] triazine (**TTT-DMAC**) (Fig. 1), with fused **TTT** as acceptor and 10*H*-phenoxazine (PXZ) and 9,9-dimethyl-9,10-dihydroacridine (DMAC) as donors. Both **TTT-PXZ** and **TTT-DMAC** not only exhibited excellent TADF properties with small ΔE_{ST} and short delay lifetime, but also exhibited AIEE properties.[42] To the best of our knowledge, this is the first report on star-shaped **TTT** derivatives with both TADF, AIEE features and used as emissive materials in OLEDs. Encouragingly, solution processed devices based on **TTT-PXZ** green emitter exhibited good performances, with an EQE of 6.2% in CzSi doped film.

Experimental

Materials

The intermediates 4-(10*H*-phenoxazin-10-yl)benzonitrile (**PXZ-BN**) and 4-(9,9-dimethylacridin-10(9*H*)-yl)benzonitrile (**DMAC-BN**) were synthesized according to reported literature.[43,44] Cyanuric chloride, PXZ and DMAC were purchased from commercial sources and used as received.

Synthesis

Synthesis of 10-(4-(2*H*-tetrazol-5-yl)phenyl)-10*H*-phenoxazine (PXZ-TZ). A mixture of **PXZ-BN** (3.70 g, 13.01 mmol), NaN_3 (1.27 g, 19.52 mmol) and NH_4Cl (0.90 g, 16.92 mmol) in DMF (20 mL) was heated at 120 °C for 36 h. After cooling down to room temperature, DMF was removed in rotavapor. After that the water was poured into mixture and extracted 3 times with 50 mL of ethylacetate. Subsequently, the collected organic phase was washed with saturated salt water and dried over anhydrous Na_2SO_4, filtered and concentrated under reduced pressure. The crude product was recrystallised with DCM to obtain a white solid (3.83 g, yield: 90%). ^{1}H NMR (500 MHz, DMSO-D_6) δ (ppm): 8.32 (dd, $J = 2$ Hz, $J = 4.5$ Hz, 2H), 7.69 (dd, $J = 2$ Hz, $J = 4.5$ Hz, 2H), 6.66–6.78 (m, 6H), 5.95 (dd, $J = 1.5$ Hz, $J = 6$ Hz, 2H). ^{13}C NMR (DMSO-D_6, 125 MHz) δ (ppm): 113.3, 115.5, 121.8, 123.8, 125.1, 129.8, 131.6, 133.5, 140.7, 143.2, 155.5. HRMS (ESI): *m*/*z* $[M]^+$ calcd for $C_{19}H_{13}N_5O^+$: 327.1120; found: 327.1129.

Synthesis of 10-(4-(2*H*-tetrazol-5-yl)phenyl)-9,9-dimethyl-9,10-dihydroacridine (DMAC-TZ). A similar procedure to **DMAC-TZ** was followed, but with **DMAC-BN** (1.58 g, 5.09 mmol) to replace 4-(10*H*-phenoxazin-10-yl)benzonitrile (**PXZ-BN**). After concentration of the solvent in rotavapor, the residue was recrystallised with DCM to obtain a white solid (1.53 g, yield: 85%). ^{1}H NMR (500 MHz, DMSO-D_6) δ (ppm): 8.34 (dd, $J = 2$ Hz, $J = 4$ Hz, 2H), 7.62 (dd, $J = 2$ Hz, $J = 4.5$ Hz, 2H), 7.51 (dd, $J = 1.5$ Hz, $J = 6$ Hz, 2H), 6.91–7.01 (m, 4H), 6.22 (dd, $J = 1$ Hz, $J = 7$ Hz, 2H), 1.64 (s, 6H). ^{13}C NMR (125 MHz, DMSO-D_6) δ (ppm): 31.3, 35.8, 113.9, 121.0, 125.3, 125.7, 126.7, 129.9, 130.1, 132.1, 140.2, 143.0, 155.9. HRMS (ESI): *m*/*z* $[M + H]^+$ calcd for $C_{22}H_{20}N_5^+$: 354.1713; found: 354.1723.

Synthesis of 3,7,11-tris(4-(10*H*-phenoxazin-10-yl)phenyl)tris[1,2,4]triazolo-[1,3,5]triazine (TTT-PXZ). A mixture of **PXZ-TZ** (1.90 g, 5.81 mmol), cyanuric chloride (0.32 g, 1.76 mmol) and anhydrous K_2CO_3 (4.98 g, 36 mmol) in 20 mL 1,4-dioxane was kept under vigorous stirring and reflux for 24 h. The hot mixture was filtered on Büchner funnel and washing with CH_2Cl_2 (3 × 20 mL). Subsequently, the collected organic phase was washed with water, saturated salt water and dried over anhydrous Na_2SO_4, filtered and concentrated under reduced pressure. The crude product was purified by column chromatography with petroleum ether/CH_2Cl_2 (v/v = 2/1) as the eluent. Finally, **TTT-PXZ** was obtained as a yellow powder (0.84 g, yield: 50%). ^{1}H NMR (500 MHz, DMSO-D_6) δ (ppm): 8.37 (d, $J = 8.5$ Hz, 6H), 7.79 (dd, $J = 2$ Hz, $J = 4.5$ Hz, 6H), 6.74–6.81 (m, 18H), 6.05 (m, 6H). ^{13}C NMR (125 MHz, DMSO-D_6) δ (ppm): 113.4, 115.6, 121.9, 123.9, 124.7, 130.8, 132.9, 133.5, 141.4, 142.1, 143.3, 148.6. HRMS (ESI): *m*/*z* $[M]^+$ calcd for $C_{60}H_{36}N_{12}O_3^+$: 972.3033; found: 972.3074.

Synthesis of 3,7,11-tris(4-(9,9-dimethylacridin-10(9*H*)-yl)phenyl)tris[1,2,4]triazolo-[1,3,5]triazine(TTT-DMAC). A similar procedure to **TTT-DMAC** was followed, but with 10-(4-(2*H*-tetrazol-5-yl)phenyl)-9,9-dimethyl-9,10-dihydroacridine (**DMAC-TZ**) (1.0 g, 2.82 mmol) to replace 10-(4-(2*H*-tetrazol-5-yl)phenyl)-10*H*-phenoxazine (**PXZ-TZ**). After concentration of the solvent in rotavapor, the residue was purified by column chromatography with petroleum ether/CH_2Cl_2 (v/v = 3/1) as the eluent. Finally, **TTT-DMAC** was obtained as a light green powder (0.64 g, yield: 70%). ^{1}H NMR (500 MHz, DMSO-D_6) δ (ppm): 8.41 (dd, $J = 2$ Hz, $J = 4.5$ Hz, 6H), 7.74 (dd, $J = 2$ Hz, $J = 4.5$ Hz, 6H), 7.55 (dd, $J = 2$ Hz, $J = 6$ Hz, 6H), 7.06–7.09 (m, 6H), 6.96–6.99 (m, 6H), 6.34 (dd, $J = 1$ Hz, $J = 7$ Hz, 6H), 1.67 (s, 18H). ^{13}C NMR (125 MHz, DMSO-D_6) δ (ppm): 31.2, 35.7, 113.9, 121.0, 124.4, 125.6, 126.6, 130.1, 131.2, 132.8, 140.0, 142.2, 143.7, 148.8. HRMS (ESI): *m*/*z* $[M + H]^+$ calcd for $C_{69}H_{55}N_{12}^+$: 1051.4667; found: 1051.4885.

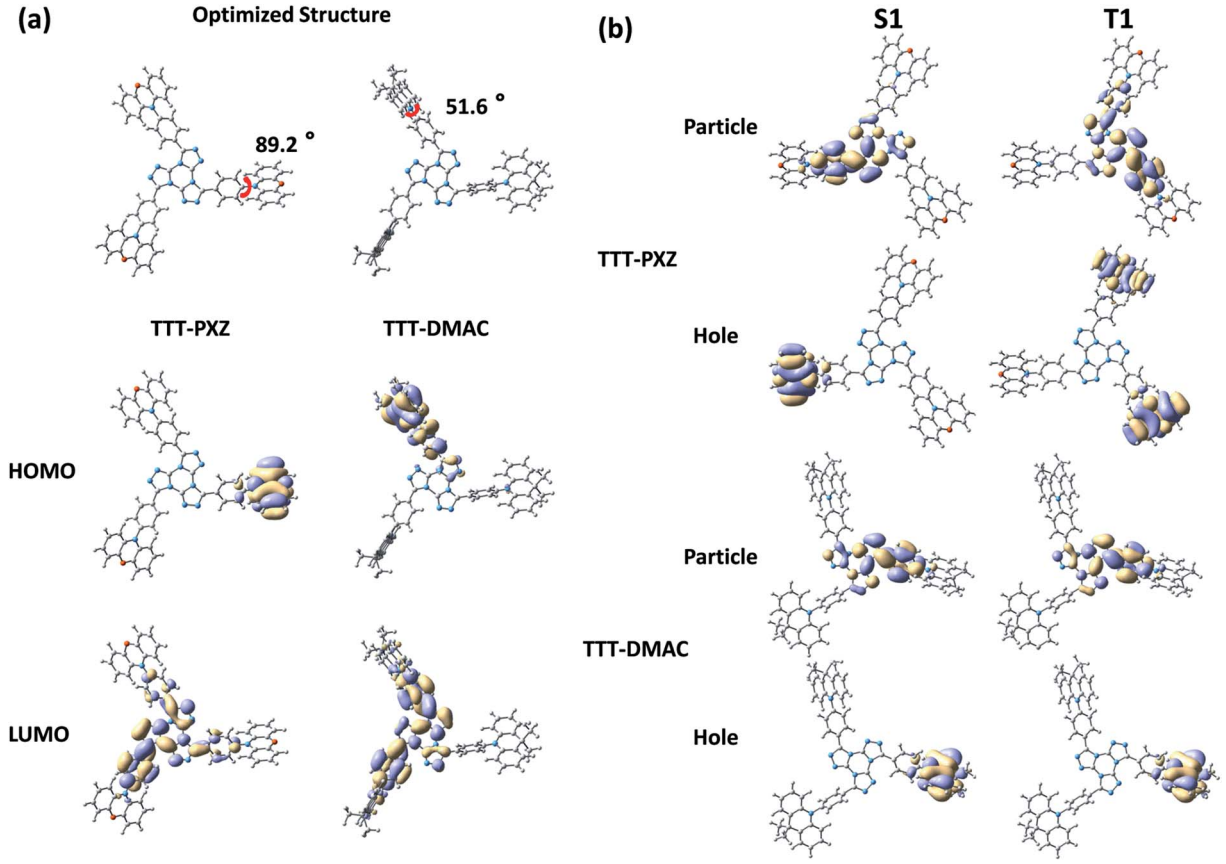

Fig. 1 The optimized geometric structures and DFT simulation of ground and excited states of TTT-PXZ and TTT-DMAC. (a) Optimized geometric structures and distribution of HOMO and LUMO, (b) natural transition orbitals (NTOs) of the hole-particle contribution for these two compounds at S_1 and T_1 excited state.

Results and discussion

Synthesis and thermal properties

The synthetic route for the preparation of two **TTT** based star-shaped molecules is depicted in Scheme 1. Target compounds of **TTT-PXZ** and **TTT-DMAC** were synthesized by Huisgen original procedure, where threefold reaction of corresponding tetrazoles precursors of **PXZ-TZ** and **DMAC-TZ** with cyanuric chloride produced the tetracyclic tris[1,2,4]triazolo[1,3,5] triazine derivatives in high yields, respectively.[39] Both target compounds can be synthesized in large amount which will benefit further commercialization. Their chemical structures were established by ^{1}H NMR, ^{13}C NMR spectroscopy and high-resolution mass spectrometry. **TTT-PXZ** possesses high thermal decomposition temperature (T_d, corresponding to 5% weight loss) of 428 °C than 241 °C of **TTT-DMAC** (Fig. S9(a)† in ESI and Table 1). The differential scanning calorimetry (DSC) traces disclose that there is no glass transition temperatures found in second heating cycles for both the emitters [Fig. S11(b) and (c)†]. This outcome points out that both compounds would be thermally stable and durable in the OLEDs application.

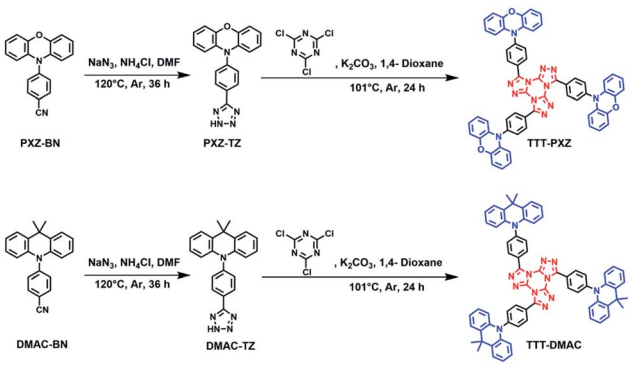

Scheme 1 The synthetic routes for TTT-PXZ and TTT-DMAC.

Electrochemical properties

Using cyclic voltammetry (CV), the electrochemical properties of the two emitters were investigated. The CV curves of both the emitters show oxidation process corresponding to the oxidation process of electron donor PXZ and DMAC unit, respectively. The HOMO levels of **TTT-PXZ** and **TTT-DMAC** were estimated to be −5.38 eV and −5.61 eV, respectively (Table 1, Fig. S14†), providing that stronger electron donating ability of PXZ drives shallower HOMO level compared to DMAC which results in red shifted emission of **TTT-PXZ** compared to **TTT-DMAC**. LUMO levels of **TTT-PXZ** and **TTT-DMAC** were determined from their

Table 1 Thermal, electrochemical and TD-DFT calculation data for TTT-PXZ and TTT-DMAC

Compound	HOMO/LUMO[a] (eV)	HOMO/LUMO[b] (eV)	S_1[b] (eV)	T_1[b] (eV)	ΔE_{ST}[b] (eV)	T_d[c] (°C)
TTT-PXZ	−5.38/−2.65	−4.77/−2.15	2.33	2.32	0.01	428
TTT-DMAC	−5.61/−2.66	−4.97/−1.38	2.70	2.66	0.04	241

[a] Obtained from cyclic voltammograms in CH_3CN solution. [b] Calculated. [c] Obtained from TGA measurements.

HOMO levels and optical bandgaps and come around −2.65 and −2.66 eV, respectively. The favorable HOMO/LUMO levels of both emitters might give an idea of selecting suitable hole and electron injection materials as well as adjacent transporting layers in OLEDs.

Theoretical simulations

We are curious to know how these two molecules **TTT-PXZ** and **TTT-DMAC** obtain their geometrically optimized structure as well as HOMO and LUMO distribution in their ground state. Density functional theory (DFT) based on B3LYP-D3(BJ)/def2-SVP (Fig. 1a) was carried out and provided valuable insights.[47] In both molecules, HOMOs are mostly distributed in donor units (PXZ or DMAC) and partially on the linking phenyl bridge resulting from the electron-donating properties of nitrogen. LUMOs act a little different. LUMO of **TTT-DMAC** extents more on the phenyl bridge compared to **TTT-PXZ** which may cause large overlap between HOMO and LUMO. Thus, charge transfer (CT) state will be weakened in **TTT-DMAC**. Further, the dihedral angle between PXZ and the phenyl bridge in case of **TTT-PXZ** is 89.2°, which is much larger than that of **TTT-DMAC** (51.6°). Therefore, it is quite obvious that **TTT-PXZ** is more twisted than **TTT-DMAC**, resulting in more efficient frontier molecular orbital (FMO) separation in the case of **TTT-PXZ**. The above results indicate that **TTT-PXZ** may possess better TADF properties than **TTT-DMAC**.

To further gather the information of the excited states, time-dependent density functional theory (TD-DFT) based on PBE0/def2-SVP was used to determine the distribution of natural transition orbitals (NTOs) as well as the values of ΔE_{ST} of **TTT-PXZ** and **TTT-DMAC** (Fig. 1b, Table 1). Particle NTOs for both compounds are located on **TTT** unit for both S_1 and T_1. While, hole NTOs are mainly spread on the respective donor moieties. Multiple distribution of hole NTO of T_1 of **TTT-PXZ** is found. This multiple D–A interaction of **TTT-PXZ** between donor and acceptor would stabilize the CT state as well as large transitional integral for a high radiative rate.[5] Moreover, both the molecules display small ΔE_{ST} of 0.01 eV and 0.04 eV for **TTT-PXZ** and **TTT-DMAC**, respectively, which results from the efficient FMO separation as shown in Fig. 1b and Table 1. Slightly large ΔE_{ST} value of **TTT-DMAC** also confirms weaker CT state formed compared to **TTT-PXZ**. Overall, we can conclude that both molecules may demonstrate good TADF characteristics.

Photophysical properties

To evaluate the optical properties, photophysical characterization of the target compounds were performed. The photophysical properties of the star-shaped molecules **TTT-PXZ** and **TTT-DMAC** in solution as well as 9-(4-*tert*-butylphenyl)-3,6-bis(triphenylsilyl)-9*H*-carbazole (CzSi) (5 wt%) doped film are depicted in Table 2, Fig. 2 and 3. Absorption spectra in dilute toluene demonstrate broad characteristic band at 394 and 358 nm for **TTT-PXZ** and **TTT-DMAC**, respectively, assigned to intramolecular charge transfer (ICT). The ICT band slightly red shifted for **TTT-PXZ** compared to **TTT-DMAC** due to stronger electron donating ability of PXZ over DMAC. The shoulder near 322 nm for **TTT-PXZ** belongs to n–π* transition. No absorption was detected around the same region for **TTT-DMAC** due to the absence of oxygen atom that possesses lone pair electrons of the corresponding donor unit. The absorption band peaked 290 nm originated from π–π* transition for both the emitters (Fig. 2a and Table S2†). Emission spectra of **TTT-PXZ** and **TTT-DMAC** in dilute toluene solution showed green emission at 522 nm and sky-blue emission at 468 nm with clear ICT character proved by solvatochromism experiment (Fig. S12, Tables S1 and S2†). Similar trends were observed for neat films for both emitters (Fig. 2b and Table S2†). When compared to the solution emission spectra, emission of **TTT-PXZ** in neat film blue-shifted 6 nm, whereas **TTT-DMAC** in neat films red-shifted 10 nm. The interesting aggregation induced blue-shifted emission (AIBSE) of **TTT-PXZ** was ascribed to lower reorganization energies in aggregates than in the solution state, the dearth of π-

Table 2 Photophysical characterization for two emitters of TTT-PXZ and TTT-DMAC

Compound	λ_{PL}[a] (nm)	S_1[b] (eV)	T_1[c] (eV)	ΔE_{ST}[d] (eV)	τ_p[e] (ns)	τ_d[e] (μs)	Φ_{PL}[f] (%)	Φ_p/Φ_d[g] (%)	k_r[h] (10^7 s^{-1})	k_{ISC}[h] (10^7 s^{-1})	k_{RISC}[h] (10^6 s^{-1})
TTT-PXZ	522	2.71	2.64	0.07	36.2	4.2	39.5	3.5/36.0	0.098	2.55	2.69
TTT-DMAC	468	2.94	2.74	0.20	49.5	4.6	21.4	1.9/19.5	0.038	1.83	2.44

[a] Measured in doped CzSi films (5 wt%) at room temperature. [b] Calculated from the onset of the fluorescence spectra of two emitters doped into CzSi films (5 wt%) at room temperature. [c] Calculated from the onset of the phosphorescence spectra of two emitters doped into CzSi films (5 wt%) at room temperature. [d] $\Delta E_{ST} = S_1^c - T_1^d$. [e] The prompt and delayed fluorescence lifetimes of two emitters doped into CzSi films (5 wt%) at room temperature. [f] The total PLQYs of two emitters doped into CzSi films (5 wt%) under oxygen free condition at room temperature. [g] The prompt and delayed PLQY under oxygen free conditions in CzSi host film. [h] Rate constant of radiative, intersystem crossing and reverse intersystem crossing process in CzSi host film.

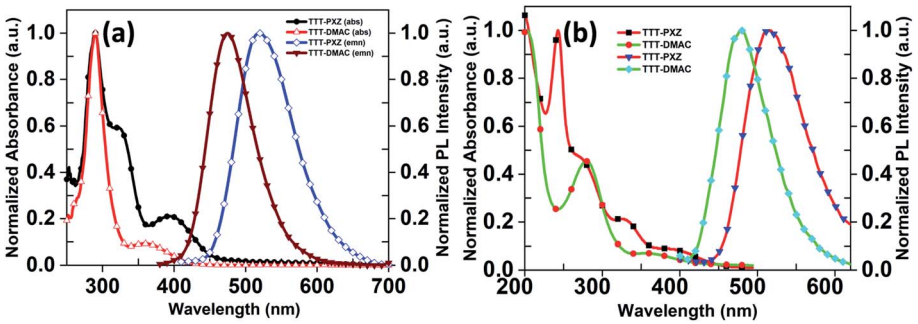

Fig. 2 (a) UV-vis and fluorescence spectra of TTT-PXZ and TTT-DMAC in 10^{-5} M toluene solution, (b) in spin coating film.

stacking due to the highly twisted structure, and weak intermolecular interactions in the solid state.[45] On the contrary, the less twisted structure of **TTT-DMAC** than **TTT-PXZ**, promotes some extent of π-stacking and intermolecular interactions, resulting in aggregation induced red-shifted emission.[46]

Fluorescence and phosphorescence spectra were carried out for both the emitters with doping concentration of 5 wt% in CzSi film recorded at 300 K and 77 K. From the onset of fluorescence and phosphorescence spectra [Fig. 3(c) and (d)], S_1/T_1 were calculated to be 2.71/2.64 eV for **TTT-PXZ** and 2.94/2.74 eV for **TTT-DMAC**, respectively. Therefore, the respective ΔE_{ST} can be calculated to be 0.07 and 0.20 eV. The low ΔE_{ST} value of **TTT-PXZ** confers it on fast RISC process compared to **TTT-DMAC** which exhibited significantly larger ΔE_{ST} (Table 2). The total PLQYs (Φ_{PL}) of **TTT-PXZ** and **TTT-DMAC** doped into 5 wt% CzSi films were measured to be 40% and 21% under argon conditions, respectively. The more twisted D–A structure of **TTT-PXZ** with small ΔE_{ST} delivered high contribution of TADF.

To gain further insight into the photophysical kinetics of two emitters, transient photoluminescence (PL) decay profile was carried out in toluene (10^{-5} M) as well as in CzSi (5 wt%) doped films. Both **TTT-PXZ** and **TTT-DMAC** illustrate double exponential decay curve under free atmosphere accompanied by prompt and delayed fluorescence lifetimes of 36.2 ns/4.2 μs and 49.5 ns/4.6 μs, respectively (Fig. 3a and b). *Via* analyzing the life time decay curve of both the emitters in 5 wt% CzSi doped film, the kinetics parameters *i.e.*, rate constants of prompt (k_p), delayed (k_d) fluorescence, radiative decay (k_r), ISC (k_{ISC}) and RISC (k_{RISC}) process can be calculated by using the equation as shown in ESI† and summarized in Table 2. The rate constant of radiative decay (k_r) and RISC (k_{RISC}) of **TTT-PXZ** are significantly higher than those of **TTT-DMAC**.

Both the emitters **TTT-PXZ** and **TTT-DMAC** were further tested for AIEE behavior in THF/water with various water fractions (f_w) from 0 to 80% (Fig. S13†). The fluorescence intensity increases many fold when the water fraction f_w reaches to 80%, signifying the AIEE behaviors of both the emitters (Fig. S13†).[42] Obviously, this enhancement of emission intensity is most likely due to the formation of aggregates. Generally, the planar π-conjugated star-shaped molecule undergoes ACQ due to intermolecular π–π stacking which is detrimental for device performance. Fortunately, twisted D–A structural design not only favors TADF but also induces AIEE features by cutting down the intermolecular π–π stacking.

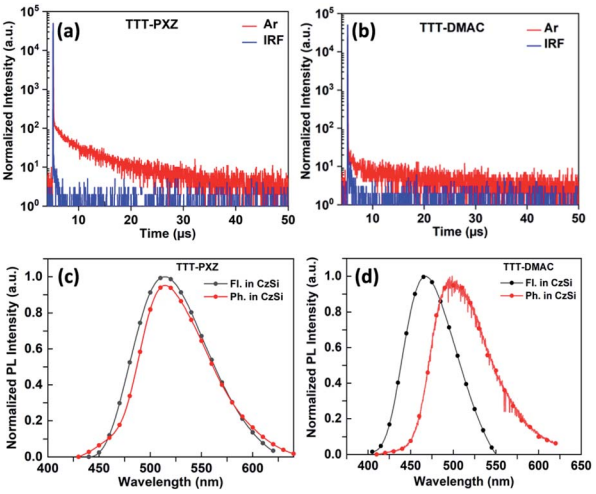

Fig. 3 Transient photoluminescence decay curves of (a) TTT-PXZ, (b) TTT-DMAC in CzSi doping film (5 wt%) under oxygen free condition. Fluorescence spectra at 300 K and phosphorescence spectra at 77 K of (c) TTT-PXZ and (d) TTT-DMAC doped into CzSi films (5 wt%).

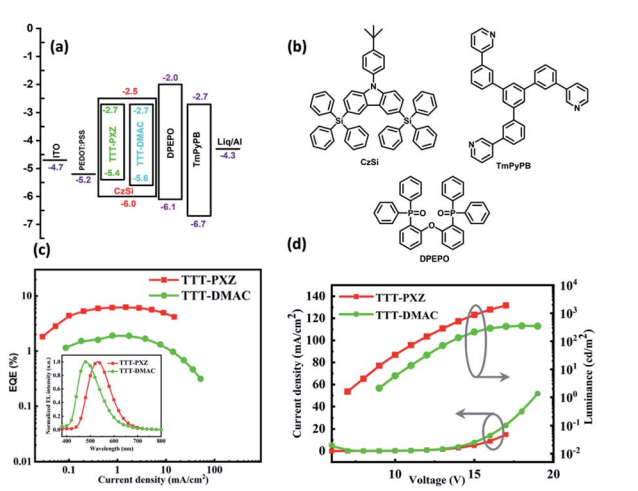

Fig. 4 (a) The energy level diagrams and (b) chemical structures of the materials used in the devices. (c) External quantum efficiency–current density curves; inset. (d) The EL spectra of devices. (e) Current density *versus* voltage *versus* luminance.

Table 3 Electroluminescence performance data of OLEDs

Emitter	V_{10}[a] [V]	EQE[b,c] [%]	CE_{max}[b] [cd A^{-1}]	PE_{max}[b] [lm W^{-1}]	λ_{max}[d] [nm]	CIE[e] (x, y)
TTT-PXZ	8.7	6.2/5.3	19.2	5.2	530	(0.32, 0.52)
TTT-DMAC	10.6	1.9/—	4.1	1.1	480	(0.19, 0.29)

[a] Voltage in the luminance of 10 cd m^2. [b] Maximum external quantum efficiency (EQE), maximum current efficiency (CE), maximum power efficiency (PE). [c] External quantum efficiency at 1000 cd m^2. [d] Peak emission wavelength of the EL spectra. [e] The CIE coordinates.

Electroluminescent properties

The detail photophysical studies encourage that both the emitters with doping concentration of 5 wt% in CzSi film can be used as emitters in OLEDs. To substantiate that, solution processed OLEDs with device configuration of ITO/PEDOT:PSS (35 nm)/CzSi: 5 wt% emitters (50 nm)/DPEPO (10 nm)/TmPyPB(50 nm)/Liq(1 nm)/Al were fabricated, where 1,3,5-tri(*m*-pyrid-3-yl-phenyl)benzene (TmPyPB) were applied as electron transport materials, bis[2-(diphenylphosphino)phenyl] ether oxide (DPEPO) were used as electron transport material/exciton blocking layer and CzSi was served as the host matrix due to its wide band gap of 3.5 eV. The schematic diagram of the device design and the energy levels of the materials are depicted in Fig. 4. Table 3 summarizes the performance data of the devices. The current density–voltage–luminance (*J–V–L*) characteristics of fabricated OLEDs are shown in Fig. 4d. The device performance based on **TTT-PXZ** was observed with high luminance 1898 cd m^{-2}, maximum current efficiency 19.2 cd A^{-1}, power efficiency 5.2 lm W^{-1} and maximum external quantum efficiency 6.2% combined with slow efficiency roll-off 14.5% at high luminance of 1000 cd m^{-2}. The device based on **TTT-DMAC** exhibited maximum luminance 346.6 cd m^{-2}, maximum current efficiency 4.1 cd A^{-1}, power efficiency 1.1 lm W^{-1} and maximum external quantum efficiency 1.9% as shown in Table 3. The improvement of device performance based on **TTT-PXZ** can be credited to its high PLQY, fast RISC process (Table 2). In addition, slow efficiency roll-off of device based on **TTT-PXZ** may be due to shorter lifetime of delayed component. Furthermore **TTT-PXZ** emits green emission with peak at 530 nm and Commission Internationale de I'Eclairage (CIE) coordinates of (0.32, 0.52), while **TTT-DMAC** based device emits in the sky blue region with peak at 480 nm and CIE coordinates of (0.19, 0.29) (Table 3). The utilization of electrical exciton (UE) for both the devices calculated from equation UE = EQE/(PLQY × η_{out}), where η_{out} is out-coupling efficiency (~0.2–0.3), are 57–86% and 30–44% (without applying light out-coupling source), respectively. Both UEs are higher than 25% limitation due to the efficient TADF feature.

In brief, the device performance based on **TTT-PXZ** was quite better than device based on **TTT-DMAC** which give assurance that by slight alteration of molecular structure in terms of choosing suitable rigid donor which not only increases the efficiency of exciton harvesting, but also provides a new prospect for the design of new kinds of efficient TADF emitters based on this unexplored fused tetracyclic rigid tris[1,2,4]triazolo[1,3,5]triazine core.

Conclusions

In conclusion, two new star-shaped D_3–A emitters (**TTT-PXZ** and **TTT-DMAC**) have been designed and synthesized by connecting donor PXZ and DMAC in three symmetrical arms with tris[1,2,4]triazolo[1,3,5]triazine acceptor *via* phenyl bridges. Theoretical simulation revealed that **TTT-PXZ** take a highly twisted conformation as compared to **TTT-DMAC**, resulting in more efficient FMO separation and smaller ΔE_{ST}. Consequently, **TTT-PXZ** showed more DF component and delivered higher PLQY than **TTT-DMAC**. Encouragingly, economically feasible solution processed doping device based on **TTT-PXZ** green emitters exhibited decent performances, with an external quantum efficiencies (EQEs) of up to 6.2%. These results make it evident that the tris[1,2,4]triazolo[1,3,5]triazine moiety is a promising rigid acceptor for efficient TADF emitters.

Conflicts of interest

There are no conflicts to declare.

Acknowledgements

This work was supported by Shenzhen Science and Technology Program (KQTD20170330110107046), the National Natural Science Foundation of China (No. 51803125 and 91833304), and Science and Technology Innovation Commission of Shenzhen (JCYJ20180507182244027). We thank the Instrumental Analysis Center of Shenzhen University for analytical support.

References

1 H. Uoyama, K. Goushi, K. Shizu, H. Nomura and C. Adachi, *Nature*, 2012, **492**, 234.
2 E. Ayataka, M. Ogasawara, A. Takahashi, D. Yokoyama, Y. Kato and C. Adachi, *Adv. Mater.*, 2009, **21**, 4802.
3 Z. Yang, Z. Mao, Z. Xie, Y. Zhang, S. Liu and J. Zhao, *Chem. Soc. Rev.*, 2017, **46**, 915.
4 Y. Tao, K. Yuan, T. Chen, P. Xu, H. Li, R. Chen, C. Zheng, L. Zhang and W. Huang, *Adv. Mater.*, 2014, **26**, 7931.
5 H. Tanaka, K. Shizu, H. Nakanotani and C. Adachi, *Chem. Mater.*, 2013, **25**, 3766.
6 X. Cai, D. Chen, K. Gao, L. Gan, Q. Yin, Z. Qiao, Z. Chen, X. Jiang and S.-J. Su, *Adv. Mater.*, 2018, **28**, 1704927.
7 J. Lee, K. Shizu, H. Tanaka, H. Nomura, T. Yasuda and C. Adachi, *J. Mater. Chem. C*, 2013, **1**, 4599.

8 F. Cherioux, L. Guyard and P. Audebert, *Chem. Commun.*, 1998, 2225.
9 J. Luo, Y. Zhou, Z.-Q. Niu, Q.-F. Zhou, Y. Ma and J. Pei, *J. Am. Chem. Soc.*, 2007, **129**, 11314.
10 W.-Y. Lai, R. Xia, Q.-Y. He, P. A. Levermore, W. Huang and D. D. C. Bradley, *Adv. Mater.*, 2009, **21**, 355.
11 C. Liu, Y. Li, Y. Zhang, C. Yang, H. Wu, J. Qin and Y. Cao, *Chem.–Eur. J.*, 2012, **18**, 6928.
12 C. Liu, Q. Fu, Y. Zou, C. Yang and J. Qin, *Chem. Mater.*, 2014, **26**, 3074.
13 L. Chen, P. Li, Y. Cheng, Z. Xie, L. Wang, X. Jing and F. Wang, *Adv. Mater.*, 2011, **23**, 2986.
14 C. Coya, C. Ruiz, Á. L. Álvarez, S. Álvarez-García, E. M. García-Frutos, B. Gómez-Lor and A. d Andrés, *Org. Electron.*, 2012, **13**, 2138.
15 X. He, L. Chen, Y. Zhao, S. C. Ng, X. Wang, X. Sun and X. Hu, *RSC Adv.*, 2015, **5**, 15399.
16 T. Huang, W. Jiang and L. Duan, *J. Mater. Chem. C*, 2018, **6**, 5577.
17 L. Duan, L. Hou, T.-W. Lee, J. Qiao, D. Zhang, G. Dong, L. Wang and Y. Qiu, *J. Mater. Chem. C*, 2010, **20**, 6392.
18 M. Shibata, Y. Sakai and D. Yokoyama, *J. Mater. Chem. C*, 2015, **3**, 11178.
19 M. Huang, Y. Li, K. Wu, J. Luo, G. Xie, L. Li and C. Yang, *Dyes Pigm.*, 2018, **153**, 92.
20 S. Gong, J. Luo, Z. Wang, Y. Li, T. Chen, G. Xie and C. Yang, *Dyes Pigm.*, 2017, **139**, 593.
21 Y. Li, T. Chen, M. Huang, Y. Gu, S. Gong, G. Xie and C. Yang, *J. Mater. Chem. C*, 2017, **5**, 3480–3487.
22 G. Xie, J. Luo, M. Huang, T. Chen, K. Wu, S. Gong and C. Yang, *Adv. Mater.*, 2017, **29**, 1604223.
23 Y. Li, G. Xie, S. Gong, K. Wu and C. Yang, *Chem. Sci.*, 2016, **7**, 5441.
24 J. Luo, S. Gong, Y. Gu, T. Chen, T. Li, C. Zhong, G. Xie and C. Yang, *J. Mater. Chem. C*, 2016, **4**, 2442.
25 J. Luo, G. Xie, S. Gong, T. Chen and C. Yang, *Chem. Commun.*, 2016, **52**, 2292.
26 Y. Zou, S. Gong, G. Xie and C. Yang, *Adv. Opt. Mater.*, 2018, **6**, 1800568.
27 R. Cristiano, J. Eccher, I. H. Bechtold, C. N. Tironi, A. A. Vieira and F. Molin, *Langmuir*, 2012, **28**, 11590.
28 Q. Niu, Y. Lu, H. Sun and X. Li, *Spectrochim. Acta, Part A*, 2013, **107**, 377.
29 P. Das, A. Kumar, A. Chowdhury and P. S. Mukherjee, *ACS Omega*, 2018, **3**, 13757.
30 Y. Wada, K. Shizu, S. Kubo, K. Suzuki, H. Tanaka, C. Adachi and H. Kaji, *Appl. Phys. Lett.*, 2015, **107**, 183303.
31 J. Jayakumar, T.-L. Wu, M.-J. Huang, P.-Y. Huang, T.-Y. Chou, H.-W. Lin and C.-H. Cheng, *ACS Appl. Mater. Interfaces*, 2019, **11**, 21042.
32 P. Ganesan, R. Ranganathan, Y. Chi, X.-K. Liu, C.-S. Lee, S.-H. Liu, G.-H. Lee, T.-C. Lin, Y.-T. Chen and P.-T. Chou, *Chem.–Eur. J.*, 2017, **23**, 2858.
33 T. Huang, D. Liu, J. Jiang and W. Jiang, *Chem.–Eur. J.*, 2019, **25**, 10926.
34 J. Li, T. Nakagawa, J. MacDonald, Q. Zhang, H. Nomura, H. Miyazaki and C. Adachi, *Adv. Mater.*, 2013, **25**, 3319.
35 S. Glang, T. Rieth, D. Borchmann, I. Fortunati, R. Signorini and H. Detert, *Chem.–Eur. J.*, 2014, **15**, 3116.
36 H. Zhao, Y. Wang, Z. Liu and B. Dai, *RSC Adv.*, 2014, **4**, 13161.
37 R. Cristiano, H. Gallardo, A. J. Bortoluzzi, I. H. Bechtold, C. E. M. Campos and R. L. Longo, *Chem. Commun.*, 2008, 5134.
38 V. A. Tartakovsky, A. E. Frumkin, A. M. Churakov and Y. A. Strelenko, *Russ. Chem. Bull.*, 2005, **54**, 719.
39 M. Sperner, N. Tober and H. Detert, *Eur. J. Org. Chem.*, 2019, 4688.
40 A. G. Dal-Bo, G. G. L. Cisneros, R. Cercena, J. Mendes, L. M. d. Silveira, E. Zapp, K. G. Domiciano, R. d. C. Duarte, F. S. Rodembusch and T. E. A. Frizon, *Dyes Pigm.*, 2016, **135**, 49.
41 D. Chai, Y. Zou, Y. Xiang, X. Zeng, Z. Chen, S. Gong and C. Yang, *Chem. Commun.*, 2019, **55**, 15125.
42 V. Anand, B. Sadhasivam and R. Dhamodharan, *New J. Chem.*, 2018, **42**, 18979–18990.
43 D. Wei, F. Ni, Z. Wu, Z. Zhu, Y. Zou, K. Zheng, Z. Chen, D. Ma and C. Yang, *J. Mater. Chem. C*, 2018, **6**, 11615.
44 N. A. Drigo, L. G. Kudriashova, S. Weissenseel, A. Sperlich, A. J. Huckaba, Md. K. Nazeeruddin and V. Dyakonov, *J. Phys. Chem. C*, 2018, **122**, 22796.
45 Q. Wu, T. Zhang, Q. Peng, D. Wang and Z. Shuai, *Phys. Chem. Chem. Phys.*, 2014, **16**, 5545.
46 Z. Zhao, S. Chen, J. W. Y. Lam, P. Lu, Y. Zhong, K. S. Wong, H. S. Kwoka and B. Z. Tang, *Chem. Commun.*, 2010, **46**, 2221.
47 W. Zeng, S. Gong, C. Zhong and C. Yang, *J. Phys. Chem. C*, 2019, **123**, 10081.